Journal of Building Engineering 73 (2023) 106836

Contents lists available at ScienceDirect

Journal of Building Engineering

journal homepage: www.elsevier.com/locate/jobe

Commercial and recycled carbon-based fillers and fibers for self-sensing cement-based composites: Comparison of mechanical strength, durability, and piezoresistive behavior

Alberto Belli [a], Alessandra Mobili [b,*], Tiziano Bellezze [b], Paulo B. Cachim [c,d], Francesca Tittarelli [b,e]

[a] Innovation Centre for Sustainable Construction (ICSC), CRH Nederland B.V., De Klencke 10-12, 1083 HL, Amsterdam, the Netherlands
[b] Department of Materials, Environmental Sciences and Urban Planning (SIMAU), Università Politecnica delle Marche, UdR INSTM, Via Brecce Bianche 12, 60131, Ancona, Italy
[c] Department of Civil Engineering, University of Aveiro, 3810-193, Aveiro, Portugal
[d] RISCO, University of Aveiro, 3810-193, Aveiro, Portugal
[e] ISAC – CNR, Via Piero Gobetti 101, 40129, Bologna, Italy

ARTICLE INFO

Keywords:
Carbon-based filler
Durability
Electrical resistivity
Piezoresistivity
Self-sensing

ABSTRACT

The possible use of industrial by-products as carbon-based fillers and/or fibers to produce Multifunctional Cement-based Composites (MCC) with piezoresistive behavior for Structural Health Monitoring (SHM) was investigated. As fillers, Used Foundry Sand (UFS) and Gasification Char (GCH) were compared with commercial Graphene Nanoplatelets (GNP). As fibers, 6 mm-long recycled carbon fibers (RCF) were compared with virgin ones. Mortars were tested in terms of mechanical strength, water absorption, microstructure, and piezoresistive behavior. UFS and GCH are more effective than GNP in decreasing the mortar electrical resistivity (−30%), total porosity (−11%), water absorption (−27%) and in increasing the compressive strength (+10%). The combination of UFS with RCF in mortars provides the best results in terms of fluidity, strength, water absorption, and piezoresistive parameters. Generally, a lower mortar resistivity, even if with lower piezoresistivity properties, allows the use of cheaper instrumentation for SHM, thanks to the lower full scale and the better correlation strength between the change in resistivity with strain.

1. Introduction

Structural Health Monitoring (SHM) allows to promptly define the onset of deterioration phenomena, maximizing the safety and service life of a structure and minimizing maintenance costs. Self-sensing is the ability of a material to perceive its own condition in terms of water saturation degree, cracking, penetration of aggressive agents, and deformations [1]. SHM methods based on self-sensing concrete are particularly advantageous in terms of sensitivity, durability, ease of installation and maintenance [2] and are implemented generally through measurements of the concrete electrical resistance [3]. In fact, the electrical resistivity of cementitious materials decreases if water [4] or aggressive ions such as chlorides and sulphates [5–8] penetrate, while it increases with carbonation [9] or cracking [10], thus allowing the precociously detection of degradation phenomena [11].

* Corresponding author.
E-mail address: a.mobili@univpm.it (A. Mobili).

https://doi.org/10.1016/j.jobe.2023.106836
Received 19 March 2023; Received in revised form 6 May 2023; Accepted 12 May 2023
Available online 13 May 2023

The self-sensing characteristic of traditional concretes can be improved through conductive additions as fillers and fibers which increase the signal-to-noise ratio (SNR) by decreasing the electrical resistance. This allows to use low-cost instrumentation to monitor the electrical resistance, giving the possibility of creating measurement networks with nodes distributed throughout the structure. Furthermore, a low electrical resistance is essential to have a piezoresistive concrete whose electrical resistivity varies with stress/strain [12–14]. The piezoresistive behavior can be exploited in SHM [15] to control the propagation of cracks [16], vehicular traffic or to create low-cost cement sensors [17] embedded in the critical points of the structure to be monitored. The fractional change of resistivity (FCR) is usually measured during the loading and unloading phases whereas the strain sensitivity is evaluated by means of the Gauge Factor (GF) defined as the ratio between the variation in electrical resistivity ($\Delta\rho/\rho$) and the deformation (ε) [17]. In addition, these conductive additions can act as reinforcements with a "crack bridging" effect in the case of fibers [18,19], and "filler effect" in the case of fillers [20].

Steel fibers reinforced cementitious materials are widely used for their excellent mechanical properties. Recent studies have shown that fibers added at 2% by volume significantly reduce the electrical resistivity of concrete [21]. The relationship between the percentage variation of electrical resistance and the applied load is linear until the appearance of cracks [22] and the GF increases with the volume of fibers up to the percolation threshold (1% by volume). Concerning different shapes, twisted fibers are the best, followed by smooth and hooked fibers [23,24]. Recently, nickel particles have also been used as fillers to fabricate self-sensing cementitious composites with good mechanical properties [25]. However, although metallic additions increase the conductivity of concrete, they also significantly increase its weight, tend to deposit due to gravity during the casting phase, and can be degraded by corrosion.

Carbon-based additions are a valid alternative [3]. Although carbon fibers (CF) [26,27] are less conductive than steel fibers, they give to cementitious composites a lower resistivity than steel fibers [28] due to their extremely thin dimensions which provide more effective electrical continuity. Both short and long carbon fibers can be used; short ones are cheaper but long fibers are more efficient as reinforcement [29]. Xi et al. [30] found a significant reduction in electrical resistivity by exceeding a certain addition threshold (percolation theory) due to the increase in electrical contact paths between the fibers. An increasing amount of CF also decreases the influence of the water/cement (w/c) ratio and the curing time on the electrical properties of concrete [31]; longer carbon fibers create more effective electrical pathways at the same volume of addition [32]. Fibers with 6 mm length have been studied by several authors [33]; Donnini et al. [34] have shown that an addition of CF equal to 3% by volume decreases the electrical resistivity of structural mortars from more than 45000 Ω·cm (reference mixture) to 110 Ω·cm. Carbon fibers are also considered to be the most effective for increasing the piezoresistive behavior of cementitious materials [35]. When short CF are added, the electrical resistivity varies with the applied load: it decreases with a longitudinal compression load ("push-in fibers"), whereas it increases in tension ("pull out fibers") [34]. Composite materials containing carbon fibers behave as stress sensors in the transverse and longitudinal directions with a usually reversible effect [36].

The use of recycled carbon fibers (RCF) instead of virgin carbon fibers (VCF) is becoming increasingly attractive for the principles of circular economy, focused on reducing the environmental impact of concrete [37]. The rapid spread of CF fabrics and panels in many industrial sectors has progressively decreased production costs and increased the volume of by-products obtained from cutting and milling manufacturing processes. These by-products can be valorized for the production of RCF [38,39]. Belli et al. [27] reported that in cement mortars the percolation threshold of VCF and RCF is between 0.1 and 0.2% by volume, with a decrease of electrical resistivity equal to 65% and 75% respectively. Brass-plated metal fibers used in their study show a lower electrical efficacy, with a percolation threshold between 0.4 and 0.8% by volume, and a decrease of electrical resistivity of only 52%.

As far as carbonaceous fillers are concerned, graphene and its derivatives are the most studied for building applications. Le et al. [40] reported that graphene nanoplatelets (GNP) make the cement mortar electrically conductive and that the electrical conductivity is not affected by the moisture content when the percolation value (the limit beyond which the additions touch) is exceeded. Du and Pang [41] found that GNP at dosages higher than the percolation value provides mortars with piezoresistive properties with reversible trend under tensile load. According to Liu et al. [42] GNP should be preferred to graphene oxide nanoplatelets (GONPs) for the production of electrical conductive mortars; moreover, a GNP dosage of 6.4% by cement mass gives cementitious composites with a stable and precise piezoresistivity, not obtained at higher (12.8%) or lower (3.2%) amounts. Carbon nanotubes (CNT) are an effective conductive filler due to their extraordinary electrical conductivity [43]. Kim et al. [44] investigated cementitious composites containing low dosages of silica fume and CNT founding improved mechanical and electrical properties owing to the decomposition of aggregated CNT in small groups. Konsta-Gdoutos and Aza [45] found the best piezoresistive sensitivity in cementitious composites containing CNT and CF at 0.1% by cement mass. According to Zhang et al. [46], multi-walled CNT increase the flexural strength of mortars and reduce electrical resistivity by up to 40% when used at 0.5% by cement mass. Jung et al. [47] stated that CNT significantly reduce the electrical resistivity of ultra-high performance concrete (UHPC) regardless of free water content. However, CNT are toxic to health as they can induce inflammatory and fibrotic reactions [48]. Nano graphite platelets (NGP) can also be used in self-sensing cementitious composites [40,49,50]; according to Huang et al. [51] the addition of NGP increases the flexural strength of cementitious composites by 82% and transforms them into highly conductive. Sun et al. [52] reported that the percolation threshold of cementitious composites filled with NGP is about 2% by volume and that the best piezoresistive behavior is obtained with 5% by volume. However, as for most nano materials, doubts remain about their harmlessness to human health [45]. Carbon black (CB) is also an attractive addition for increasing the self-sensing properties of concrete thanks to its electrical conductivity and low cost [53–55]. Wen and Chung [35] reported that both CF and CB at 15% by cement mass increase electrical conductivity in direct current (DC) but carbon fibers are more effective than carbon black. Partial replacement (50%) of carbon fibers with carbon black reduces the cost, as well as increases workability, while maintaining the same electrical conductivity. However, partial replacement reduces the piezoresistive behavior whereas the total replacement decreases the concrete electrical conductivity. According to Monteiro et al. [56] CB added to 4% by cement mass improves the mechanical performance of mortars, while between 7% and 10% it provides good piezoresistive behavior.

However, also in this case possible toxicity for human health has been reported [45].

Therefore, carbonaceous additions thanks to their high mechanical resistance, high aspect ratio (for the fibers), large specific area (for the fillers), lightness and electrical conductivity [40,57,58] allow to improve the mechanical, electrical, and durability properties of concrete [59–61]. However, commercial carbon fillers, such as GNP and CNT, are difficult to disperse in polar liquids as water due to their hydrophobic nature and high specific surface area, where Van der Waals forces create agglomerates [62,63], while an adequate dispersion of these additions in the concrete mix is a prerequisite for their effective use in cementitious composites. Furthermore, the use of these additions at an industrial level is not feasible due to their high costs, their non-eco-sustainability, and sometimes toxicity. Therefore, cheaper, eco-sustainable and easily dispersible industrial by-products, thanks to a lower specific surface, and a different chemical composition that makes them more compatible with water, should be adopted. Used foundry sand (UFS) is an industrial by-product of steel mills where it is used for molds thanks to its high thermal conductivity. It has a high silica content, but also contains carbonaceous additions and many metals [64]; the addition of UFS at 1% by binder mass reduces the electrical resistivity of hydraulic lime pastes by 65% [65] whereas at 4% by binder mass increases the electrical resistivity of cement-based mortars [66]. Gasification char (GCH) is a porous carbon-based industrial by-product obtained from the gasification of biomass to produce energy [67]. Recent studies have shown that GCH added from a minimum of 0.25% to a maximum of 1% by binder mass reduces the electrical resistivity of hydraulic lime based pastes by 65% [65]. If added at 4% by binder mass, it reduces the electrical resistivity of cementitious mortars by 42%, which is lowered further (by 80%) when combined with RCF at 0.7% on binder mass [66]. As a matter of fact, to increase the self-sensing performance CF have also been combined with fillers such as carbon black [35] and graphite [68]: the fibers form a network, while the filler fills the spaces between the fibers, thus increasing the electrical conductivity of the material.

To the best of the authors' knowledge, no studies were focused on the effect of low-cost carbon-based industrial by-products in the form of both fillers and fibers on the properties of self-sensing cement-based composites. Therefore, in this paper, commercial carbon-based fillers and fibers have been compared with industrial by-products to produce low-resistivity Multifunctional Cement-based Composites (MCC) with self-sensing behavior for SHM. As fillers, UFS and GCH were compared with GNP; as fibers, 6 mm-long virgin fibers were compared with recycled ones. Mortars manufactured both with fillers or fibers alone and in combination were tested in terms of mechanical strength, water absorption, microstructure, and piezoresistive behavior.

2. Experimental

2.1. Materials

Ordinary Portland-limestone cement (OPC) CEM II/B-L 32.5 (EN 197-1) supplied by Cimpor was used as binder whereas a medium-coarse saturated surface dry silica sand (D_{max} = 8 mm, water absorption = 2.5% by mass) was used as aggregate.

Graphene Nanoplatelets (GNP), commercially available as Pentagraph 30 (supplied by Pentachem S.r.l.), with 6–8 nm flake thickness, were used as commercial reference carbon-based filler (Fig. 1a). A char from biomasses gasification (GCH), provided by a plant located in central Italy, and a Used Foundry Sand (UFS) supplied by LA.BO S.r.l. (Italy) were employed as recycled fillers. Both GCH and UFS were supplied in coarse size; therefore, they have been ground and sieved at a d < 75 μm before their addition in mortars

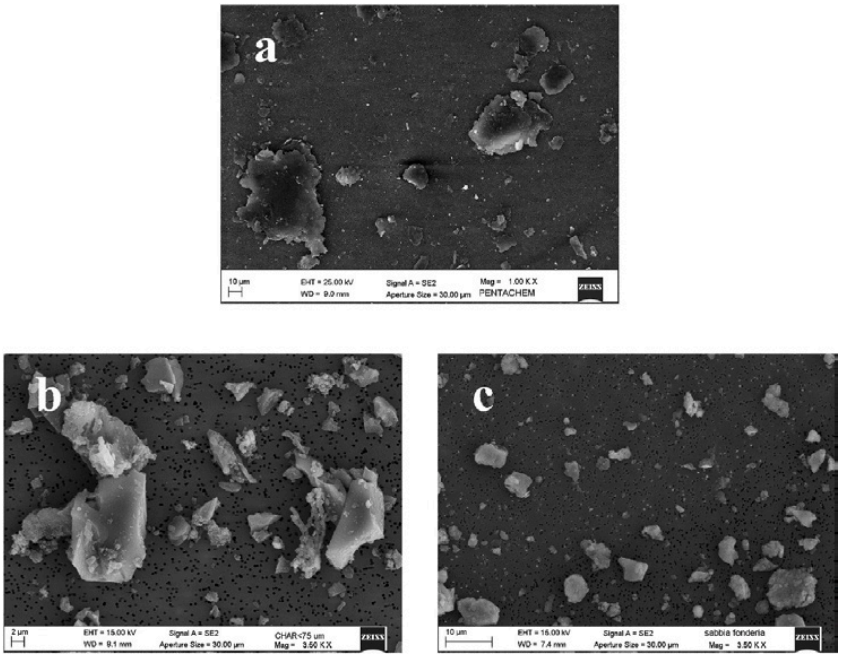

Fig. 1. SEM images of carbon-based fillers: a) GNP, b) GCH, c) UFS.

(Fig. 1b and c). The morphology of the studied carbon-based fillers is different: GNP is composed of several layers of graphene nanosheets with a foil-like and wrinkled structure, GCH is characterized by elongated particles with an irregular shape, and UFS is composed of particles with a predominant spherical shape. The full characteristics of GNP, GCH and UFS fillers are reported in Refs. [65,66] where also particles size and morphology are given.

As Carbon Fibers (CF), Virgin Carbon micro-Fibers (VCF) supplied by STW GmbH (Fig. 2a) and produced by polyacrylonitrile precursors, were compared with Recycled Carbon Fibers (RCF), supplied by Apply Carbon SA, obtained by carbon panels cutting and milling (Fig. 2b). Both types of fibers have an average length and diameter of 6.0 mm and 7.0 μm, respectively. The technical and dimensional properties of carbon-based fillers and fibers are given in Tables 1 and 2, respectively.

Carbon-based fillers were tested in 2 different dosages, i.e., 4% and 7% by cement mass, which correspond to 1% and 2% by mortar volume. Carbon fibers were added at 0.05% and 0.2% by mortar volume, since these concentrations gave good strength and conductivity to mortars in previous experimentations [27]. Hybrid filler/fiber additions were also investigated by combining 4% by cement mass of filler, i.e. 1% of mortar volume as studied in a previous work [19], with the two concentrations of fibers. A powdered polycarboxylate ether Superplasticizer (SP) MELFLUX® 4930F (produced by BASF SE) was used in order to obtain a better dispersion of fillers and fibers within the matrix [70,71]. The SP was dosed to reach at least a plastic consistence, i.e. above 140 mm according to the EN 1015-6 standard [72]. A plain mortar without fillers or fibers was also prepared as reference (REF). In total, 22 mortar mixes were manufactured as reported in Table 3.

2.2. Preparation of specimens

An aggregate/cement ratio equal to 3 and a water/cement (w/c) ratio equal to 0.5 by mass were set for the mix design. To ensure a homogeneous distribution of the fillers within the matrix, the carbon-based powders were previously dispersed in the mixing water with SP, and sonicated for 30 min by means of an ultrasonic bath [73]. At first, cement, sand, and fibers were manually mixed, then water, with fillers if present, was added to the solids and mixed in a Hobart mixer for 5 min. Fig. 3 shows the process to produce all specimens. The fresh mortars were poured into steel molds, to realize 40 mm × 40 mm × 160 mm specimens. According to the standard EN 1015-11 [74], the specimens were cured at temperature (T) = 20 ± 1 °C and relative humidity (RH) = 95 ± 5% for 7 days, and then at T = 20 ± 1 °C and RH = 65 ± 5% until testing.

2.3. Testing methods

2.3.1. Consistence of fresh mortars

To evaluate the effect of fillers and fibers on the fluidity of mortars, the fresh mixtures were characterized by means of a flow table according to the EN 1015-3 standard [75]. The fluidity of fresh mortars is measured by the consistence, which describes quantitatively the deformability of the fresh mortar when it is subjected to a certain type of stress. The flow value was measured according to the EN 1015-6 standard [72].

2.3.2. Mechanical properties

The effect of fillers and fibers on the mechanical properties of mortars was investigated by flexural (R_f) and compressive (R_c) strength tests on 40 mm × 40 mm × 160 mm mortar specimens at 28 days of curing, according to the EN 1015-11 standard [74]. For each mix, 3 specimens were tested, and the average result reported.

2.3.3. Porosity and microstructure

After 28 days of curing, the microstructure of mortars was investigated by mercury intrusion porosimetry (MIP) with a Thermo Fisher 240 Pa porosimeter, by analyzing the pore size distribution and calculating the total porosity (V_p) and the average pore diameter (d_p). The tests were performed on mortars with single addition of filler or fiber, to highlight the effects of single dosages. The porosimeter works with a measuring pressure range from 0.01 to 200 MPa; the mercury contact angle is equal to 140° and the mercury surface tension is equal to 0.48 N/m. The pore size that can be measured with this system ranges between 0.0037 and 7.5 μm; pores bigger than 7.5 μm cannot be directly measured; however, macropores greater than 1 mm can be observed visually.

2.3.4. Water absorption

The effect of fillers and fibers on the capillary water absorption was tested after 28 days of curing. The hardened specimens were cut

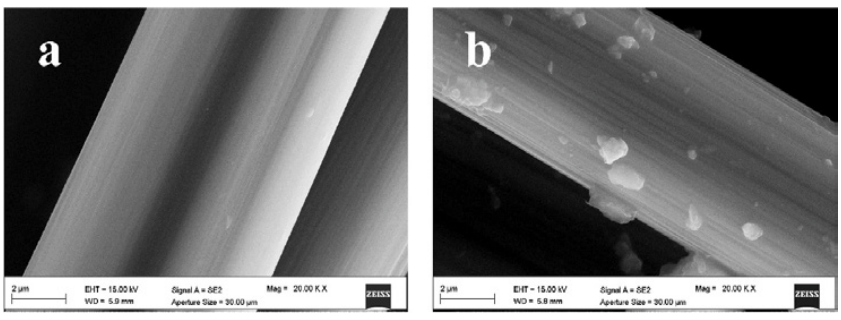

Fig. 2. SEM images of carbon fibers: a) VCF, b) RCF [69].

Table 1
Properties of carbon-based fillers (from suppliers).

	GNP	GCH	UFS
Color	Black, Grey	Black	Black
Carbon content [% by mass]	>99	>75	>30
Density [g/cm^3]	2.0 ± 0.1	2.1 ± 0.1	1.9 ± 0.1
Bulk density [g/cm^3]	0.3 ± 0.05	0.3 ± 0.05	0.8 ± 0.1
BET surface area [m^2/g]	30	76	341
Particles thickness [nm]	6–8	–	–
Young's modulus [GPa]	1000	–	–
Thermal conductivity [W/(m·K)]	3000	–	–
Electrical conductivity [S/m]	10^7	–	–

Table 2
Properties of carbon fibers (from suppliers).

	VCF	RCF
Color	Black	Black
Carbon content [% by mass]	>92	94 (>92)
Surface coating	Epoxy	Glycerol
Density [g/cm^3]	1.78	1.7–2.0
Thickness (diameter) [μm]	7.0	7.0 ± 2.0
Filament length [mm]	6.0	6.0 ± 0.5
Specific surface area [m^2/g]	0.229	–
Young's modulus [GPa]	230–250	230
Tensile strength [MPa]	4000	3500
Average resistivity [Ω·cm]	0.0015	0.0015

Table 3
Mix proportions of mortars (g/L).

Mixture	CEM	Water	Sand	GNP	GCH	UFS	Fibers		SP
							VCF	RCF	
REF	512	256	1534	–	–	–	–	–	–
GNP4	506	250	1516	20	–	–	–	–	10
GNP7	500	250	1500	35	–	–	–	–	2.3
GCH4	506	253	1517	–	20	–	–	–	0.6
GCH7	502	251	1505	–	35	–	–	–	1.1
UFS4	505	252	1514	–	–	20	–	–	1.3
UFS7	501	250	1502	–	–	35	–	–	1.3
***0.*05VCF	511	256	1533	–	–	–	0.9	–	0.1
***0.*2VCF	510	255	1530	–	–	–	3.4	–	0.5
***0.*05RCF	511	256	1533	–	–	–	–	0.9	0.3
***0.*2RCF	510	255	1529	–	–	–	–	3.7	0.6
***GNP-0.*05VCF	505	253	1514	20	–	–	0.9	–	1.1
***GNP-0.*2VCF	504	252	1510	20	–	–	3.4	–	1.9
***GNP-0.*05RCF	504	252	1512	20	–	–	–	0.9	1.7
***GNP-0.*2RCF	504	252	1512	20	–	–	–	3.7	2.4
***GCH-0.*05VCF	505	253	1515	–	20	–	0.9	–	1.1
***GCH-0.*2VCF	504	252	1512	–	20	–	3.4	–	1.3
***GCH-0.*05RCF	505	253	1515	–	20	–	–	0.9	1.1
***GCH-0.*2RCF	504	252	1512	–	20	–	–	3.7	1.4
***UFS-0.*05VCF	504	252	1511	–	–	20	0.9	–	1.7
***UFS-0.*2VCF	503	252	1509	–	–	20	3.4	–	1.9
***UFS-0.*05RCF	504	252	1510	–	–	20	–	0.9	2.0
***UFS-0.*2RCF	503	252	1508	–	–	20	–	3.7	2.0

in half to obtain 40 mm × 40 mm × 80 mm specimens dried in oven at 105 °C until constant mass. For the evaluation of short-term absorption, the cut surface of the specimens was placed in direct contact with water (for a depth of 10 mm), and the mass of the specimens was measured after 10 and 90 min (M_{10} and M_{90}, respectively). The absorption coefficient (C) was thus calculated, according to the EN 1015-18 standard [76], using Eq. (1).

$$C = 0.1 \bullet (M_{90} - M_{10}) \quad (1)$$

The absorption for longer period of time was evaluated according to the EN 15801 standard [77]. The cut surface of the specimens was placed in contact with wet sheets of blotting paper for 8 days. The weight of the specimens was measured at different time intervals, to measure the water absorption over time, until a stable and final weight (M_f) was reached. The total absorbed water Q_f was

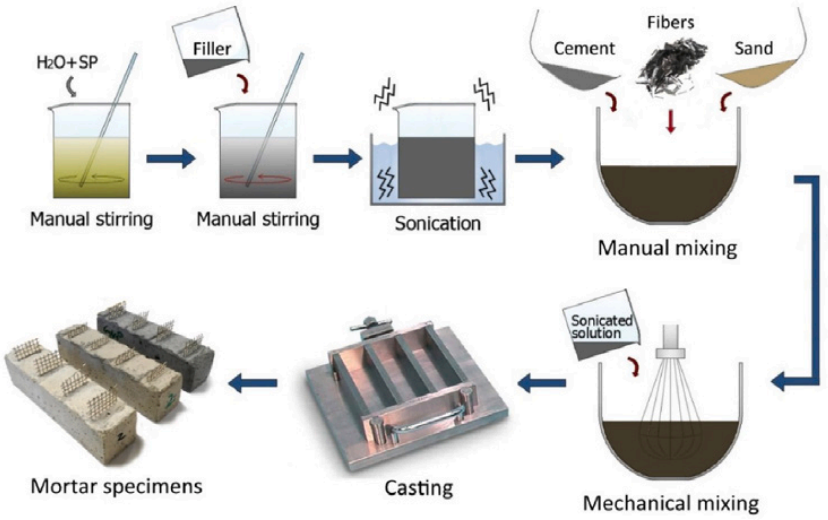

Fig. 3. Mortar specimens manufacturing process.

thus calculated using Eq. (2).

$$Q_f = \frac{(M_f - M_0)}{A} \tag{2}$$

where M_0 is the initial weight of the dry specimen and A is the wet surface (40 mm × 40 mm).

2.3.5. Piezoresistivity

Three 40 mm × 40 mm × 160 mm specimens with embedded electrodes were used for the assessment of the piezoresistive behavior of the different mixes. Four #6 stainless steel grids (with an area (A) of 30 mm × 30 mm) were used as electrodes, positioned in the specimens at a distance (l) of 40 mm (Fig. 4). For each mix, 2 specimens were tested, and the average result reported.

The evaluation of the piezoresistivity was performed by a 4-probe DC method; this setup is widely used [32,78–80] to monitor the electrical resistivity of specimens subjected to quasi-static stress cycles. An electric tension was applied to the external electrodes of the specimens by using a DC power supply PROTEK, equivalent to a current I (of at least 5 μA) measured through a 120 Ω shunt resistor. The voltage U (mV) was thus measured between the internal electrodes and recorded using a Data Taker DT80 Data Acquisition device (DAQ) [81,82]. The R and ρ values were automatically calculated by the DAQ through Eqs. (3) and (4), during the whole test.

$$\boldsymbol{R} = \frac{\boldsymbol{U}}{\boldsymbol{I}} \tag{3}$$

$$\boldsymbol{\rho} = \boldsymbol{R}\frac{\boldsymbol{A}}{\boldsymbol{l}} = \frac{\boldsymbol{U}}{\boldsymbol{I}} \bullet \frac{\boldsymbol{A}}{\boldsymbol{l}} \tag{4}$$

where A is the contact area between the electrodes and the material (30 mm × 30 mm) and l is the spacing between the inner electrodes (40 mm, Fig. 4). The axial stress was applied through a SHIMADZU AG-IC press, isolating the specimen from the press by using plastic plates. An initial load of 2 kN was applied and maintained for 2 min, until the stabilization of the ρ value was reached. Thereafter, 10 loading/unloading cycles were performed, with a maximum compressive load of 25 kN (i.e. max stress σ = 15.6 MPa, in the elastic behavior of mortars) and a loading speed of 250 N/s.

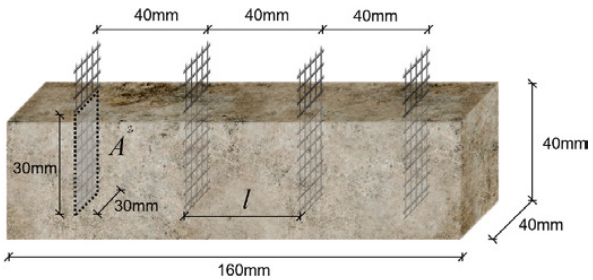

Fig. 4. Mortar specimens for piezoresistivity tests.

The axial deformation of the specimens under load was measured through a 25 mm, 120 Ω strain gauge, with a Gauge Factor (GF) = 2.07, placed in the center of the specimen. A Wheatstone bridge was used to connect the strain gauge to the DAQ, in order to obtain an instantaneous and accurate reading of the axial deformation με [73]. The test equipment, i.e. DC power supply and Shimadzu press, were also connected to the DAQ, thus simultaneously detecting the load force, strain, current, voltage, and calculating the resulting electrical resistance of the material by means of the device software. Fig. 5 shows the scheme of the experimental test setup.

According to the results, 3 parameters were used to measure the piezoresistivity properties of the composites [12,56].

The Fractional Change in Resistivity (FCR), which calculates the change in resistivity modulus Δρ over time, starting from the resistivity ρ_0, obtained by the unloaded specimen (Eq. (5)). In particular, the maximum FCR (max. Δρ) was measured at the maximum load.

$$FCR = \frac{|\rho_{(t)} - \rho_0|}{\rho_0} = \frac{\Delta\rho}{\rho_0} \tag{5}$$

The Gauge Factor (GF), also called strain sensitivity, which relates the variation in resistivity with the axial deformation ε, by Eq. (6):

$$GF = \frac{\frac{\Delta\rho}{\rho_0}}{\varepsilon} = \frac{FCR}{\varepsilon} \tag{6}$$

Lastly, the stress sensitivity (SS), which relates FCR with the applied axial stress σ (equal to 15.6 MPa), was calculated by Eq. (7):

$$SS = \frac{FCR}{\sigma} \tag{7}$$

The specimens were subjected to piezoresistivity tests after 28 days of curing, to ensure the full development of their mechanical properties, and in dry conditions (dried in oven at T = 60 °C until constant weight) in order to eliminate the influence of moisture on the electrical behavior of the composites [56].

3. Results and discussion

3.1. Consistence of fresh mortars

By carefully dosing the SP, the fluidity of all mortars was maintained similar to REF (flow value of 185 mm) with a flow value above 160 mm. Nevertheless, fillers and fibers seem to act differently on fresh mortars (Fig. 6). Concerning fibers, both VCF and RCF decrease mortar workability, as reported by Donnini et al. [34], and a higher amount of CF leads to a lower flow value [83], even in the hybrid fillers/fibers mortars. Concerning fillers, UFS leads, on average, to lower flow values, as confirmed by other studies, because of the presence of clay-impurities [84,85] and this result is obtained also when CF are present. On the contrary, GCH maintains the mortars fluidity unaltered when it is used alone but increases the mortars fluidity when coupled to CF. However, at least at these dosages, differently from fibers, fluidity is not affected by the amount of filler. In the fresh state, the main issues related to consistence were found in mortars containing GNP, especially at high concentrations (GNP7). The high hydrophobicity of graphene, related to its non-polar nature, causes inhomogeneity and segregation phenomena in the mix with consequent separation of the liquid from the solid part (bleeding), as already shown in other studies [42,86,87], and a foamy texture due to air trapping (Fig. 7).

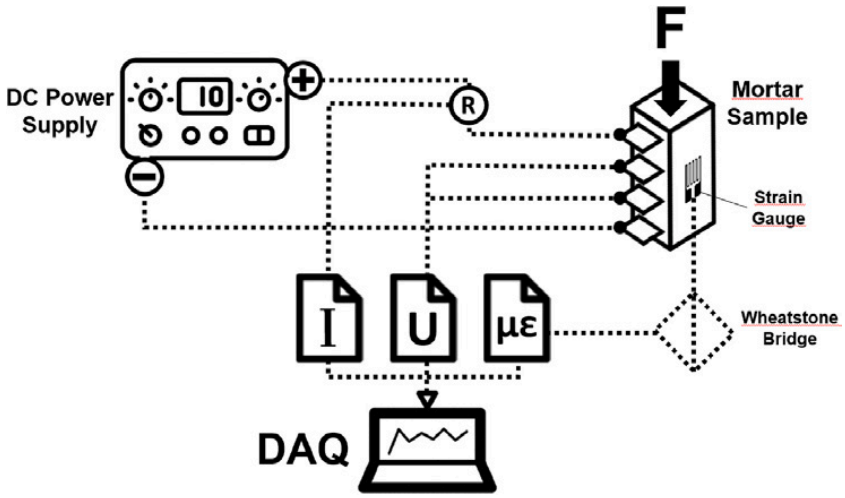

Fig. 5. Scheme of piezoresistivity tests setup. R is the shunt resistor of 120 Ω for measuring the current I between the two external grid electrodes.

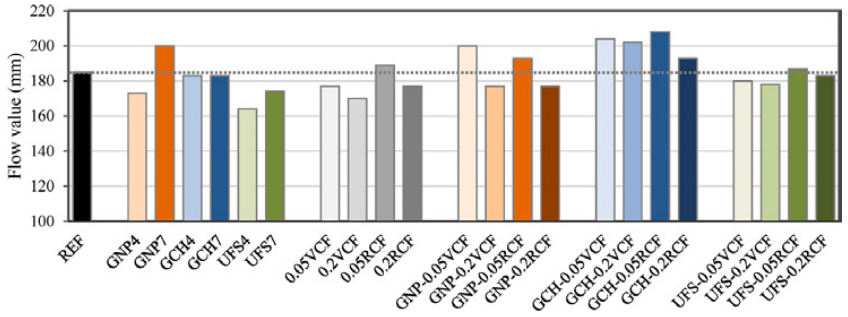

Fig. 6. Consistence of fresh mortars in terms of flow value.

Fig. 7. Fresh GNP-based mixtures (GNP7): segregation (left) and bleeding with high content of air bubbles (right).

3.2. Mechanical strength and microstructure

The mechanical performance of the composites at 28 days of curing is shown in Figs. 8 and 9 where the dashed line refers to the results obtained by the reference mortar without additions.

In general, mortars with recycled fillers show a comparable or slightly higher flexural strength than the REF mortar (Fig. 8). The mixtures with 4% GCH and UFS by mass of cement increases the flexural strength by 6% and 14%, respectively, whereas for 7% addition the R_f value slightly decreases. Indeed, at both GNP percentage additions mortars show R_f values similar to REF. Little improvements (+9%) can be observed for mortars prepared only with CF, thanks to the bridging effect of the filaments [18,19,88,89], regardless of percentage addition. Concerning hybrid filler/fibers mixes, those containing CF and GNP show slightly lower flexural strength values than REF from 3 to 9%. On the contrary, mortars manufactured with VCF and RCF at both percentage additions and GCH or UFS do not show any flexural strength improvement. Concerning the compressive strength results (Fig. 9), the lowest dosage of GCH and UFS gives the highest R_c, of 34.5 and 34.9 MPa, respectively (10–11% higher compared to REF). Moreover, also the hybrid filler/fibers mixes containing GCH and UFS show slightly higher compressive strength values (around 2 and 7%, respectively) compared to REF. The increase of mechanical strength registered by mortars containing GCH and UFS is related to the filler effect [20]. Indeed, nano/micro fillers work as nucleation sites for C–S–H [90], accelerating the degree of hydration and consequently increasing the mechanical strength of hardened compounds. Mrad and Chehab [91] reported that the porous surface of char causes the migration of water from the particles to the surrounding paste. This migration promotes cement hydration resulting in a denser and less porous interfacial transition zone (ITZ) with respect to that between sand and cement paste. On the other hand, the high content of silica in UFS would have helped in the formation of C–S–H gel [64]. Conversely, all mortars with GNP show lower R_c values than the reference mix, in particular, the R_c value drops from 31 MPa for REF to 24 MPa for GNP7 mortar (−16%). Mortars containing only VCF or RCF show slightly lower R_c values than REF (−7%). The reduction of compressive strength is visible also for mortars manufactured with both GNP and CF. It is reported that graphene nanosheets, especially graphene oxide [62,92,93], can provide the nucleation sites for

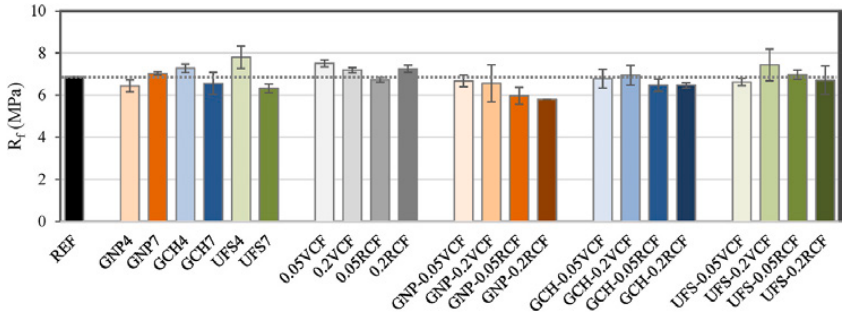

Fig. 8. Flexural strength R_f of mortars (28 days).

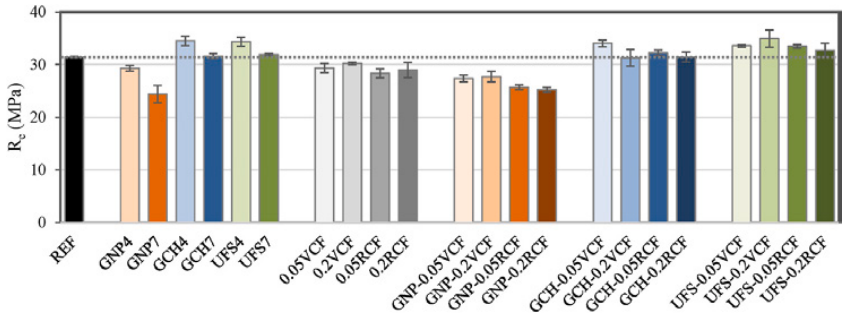

Fig. 9. Compressive strength R_c of mortars (28 days).

the growth of C–S–H, thereby resulting in enhanced mechanical properties of the hardened compounds. However, the difficulties during casting and the poor homogeneity of the fresh GNP-based mortars led to a high volume of large voids in the hardened composites, as found also in Ref. [86]. Furthermore, the hydrophobicity of GNP hinders the proper hydration of cement, and leads to a lower development of mechanical performances, as already assessed by other authors [94,95], even though the total pore volume and average pore diameter of mortars as detected by MIP are lower than the REF (Table 4). Fig. 10 shows the internal section of the specimens from some selected mixtures, in which the macropores (pores larger than 1 μm [96]) of the GNP mortars are clearly visible.

To support these results and to highlight the effect on porosity of single additions of filler and fiber, porosimetric tests were performed on the mortars with single additions. In Table 4, the effects of fillers and fibers on the microstructure of the composites are reported.

Almost all types of additions lead to a refinement of the cement paste. Both commercial (GNP) and recycled (GCH, UFS) fillers at 4% by cement mass reduce both the pore volume and size (average pore diameter d_p) and a further addition of fillers (7% by cement mass) leads to a higher reduction of pores quantity and dimension. However, the filler effect is enhanced by recycled GCH and UFS fillers, with a 9% and 11% reduction of total porosity and a 26% and 27% reduction of the average pore diameter, respectively. This proves that the micro-particles of the fillers can fill the pores and act as nucleation sites for C–S–H [97,98] improving the hydration degree of the cement, as well as the mechanical properties of composites [65,90]. The effect of CF on the microstructure of the mortars is less evident; however, the lower porosity of RCF mortars suggests that the micro-fragments that are present on the surface of the RCF (Fig. 2b) have the same effect of fillers in the matrix [27,99]. A reduction of the total volume and size of pores was also detected in mixtures containing GNP, proving that, despite the formation of large voids, the GNP addition has a refining effect on pores lower than 15 μm [100]. In fact, it is worthy to underline that the porosimeter used in this test can measure pores ranging between 0.0037 and 7.5 μm; the larger pores, although observable by visual investigation (Fig. 10), cannot be measured by this test. To support this fact, the density of the dried specimens has been reported in Table 4. The density of specimens GNP4 and GNP7 is comparable with that of REF.

3.3. Water absorption

The absorption coefficient C (short-term absorption) of mortars measured by the capillary water absorption tests is shown in Fig. 11.

Generally, almost all mortars with fillers and/or fibers show higher resistance to water absorption, compared to the plain mortar thanks to the lower total porosity; the addition of GNP or UFS reduces water absorption of about 20% whereas GCH of only 6%. Also VCF and RCF contribute to water absorption reduction. However, the combined addition of fillers and fibers entails the lowest water absorption, with a decrease of C value up to 27%. GNP, GCH, and UFS decrease the water uptake thanks to the reduced total pore

Table 4
Total porosity (V_p), average pore diameter (d_p) and dry density of mortars.

Mixtures	V_p (%)	d_p (μm)	Density (g/cm^3)
REF	17.4	0.090	2.176
GNP4	17.1	0.080	2.164
GCH4	16.5	0.075	2.191
UFS4	16.7	0.072	2.182
GNP7	16.2	0.068	2.165
GCH7	15.9	0.067	2.213
UFS7	15.5	0.066	2.207
0.05VCF	18.4	0.093	2.128
0.2VCF	15.7	0.078	2.146
0.05RCF	13.9	0.103	2.084
0.2RCF	16.5	0.078	2.118

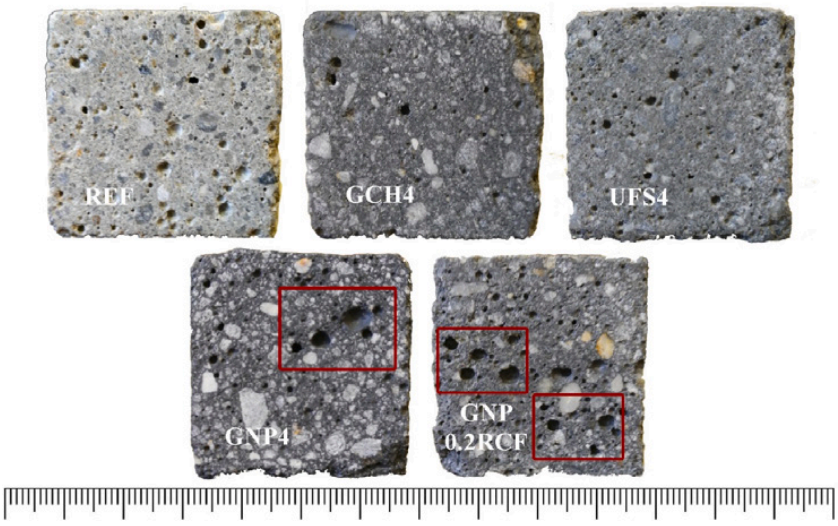

Fig. 10. Comparison of the internal section of different mortar mixes with voids highlighted in red in GNP mortars (the scale is in mm). (For interpretation of the references to colour in this figure legend, the reader is referred to the Web version of this article.)

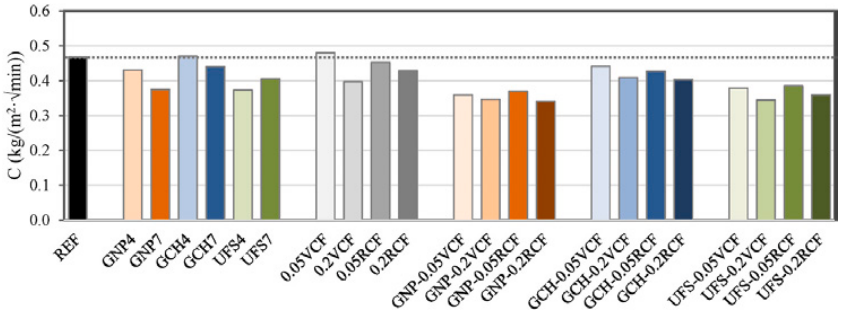

Fig. 11. Water absorption coefficient (C) of mortars.

volume and average pore diameter compared to REF (Table 4). In particular, the significant decrease of water absorption by GNP addition compared to GCH is also due to its hydrophobic nature and barrier properties [101,102] related to the reduced average pore diameter (Table 4). On the other hand, the lower water absorption of mortars with UFS compared to GCH is related to the lower carbon content of UFS (Table 1). Indeed, the higher the carbon content of the addition, the higher the water absorption [103]. As found in a previous study [65], increasing GNP and GCH content, the water suction decreases; conversely, increasing UFS content the water suction increases, because of the increased presence of clay impurities in the filler, which are known to be hydrophilic.

In the long-term absorption (Fig. 12), the effect of fillers and fibers is mitigated. In the first period of water contact, the absorption is less in mortars loaded with GNP and UFS; however, after 2 days (corresponding to about 400 $\sqrt{s}$), all mortars show water absorption values comparable to REF. On average, UFS mortars have a higher water penetration resistance than GNP and GCH and the amount of absorbed water is not related to the fillers or fibers dosage.

3.4. Piezoresistivity

The electrical resistivity ρ_0 and the maximum strain ε needed to calculate the piezoresistive parameters are reported in Fig. 13a and Table 5, respectively. The piezoresistive behavior of the different mortars subjected to 10 load/unload cycles is compared in Fig. 13b in terms of FCR and in Table 5 in terms of GF and SS parameters (section 2.3.5). Most of the mixtures show a detectable piezoresistive behavior, with detectable FCR, GF, and SS values, including the REF mortar. The mixes not showing any piezoresistive behavior (not detectable FCR, GF, and SS values) are generally those those with a high initial DC resistivity ρ_0 (>3000–4000 Ω m, Fig. 13a); specimens with high resistivity requires a very high voltage during the measurements, and this makes the system not sensitive to the variations in electrical resistivity due to deformation.

Fig. 14 shows the change in resistivity under strain of some representative mortars with piezoresistive behavior where also the corresponding correlations between FCR and strain are reported. A lower data dispersion means a higher correlation strength between FCR and strain, whereas the slope of the FCR and strain correlation line reflects the GF (the higher the slope, the higher the GF).

Concerning fillers, UFS and GCH are more effective than GNP to decrease the DC electrical resistivity of mortars (Fig. 13a), but the

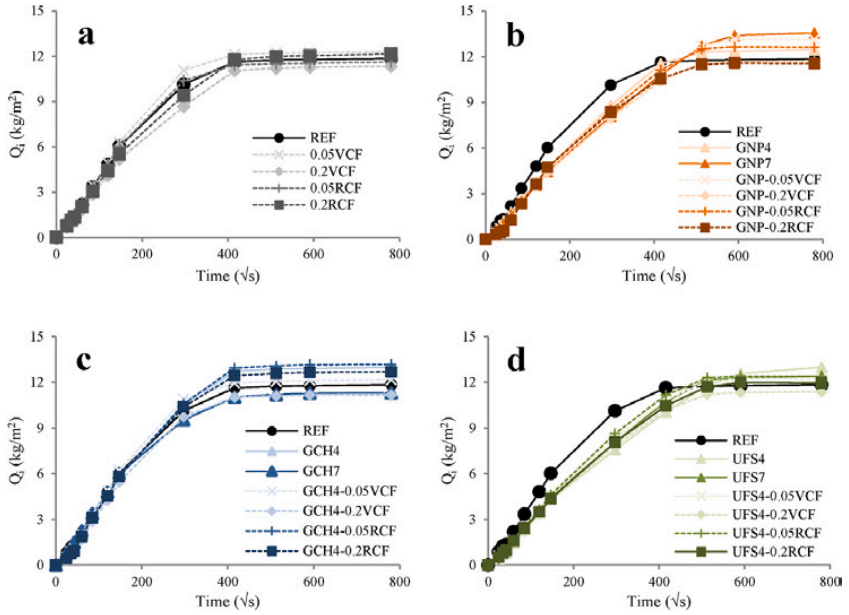

Fig. 12. Water absorbed per unit area Q_i (long period): A) REF and carbon fibers, B) GNP and GNP-CF, C) GHC and GCH-CF, D) UFS and UFS-CF

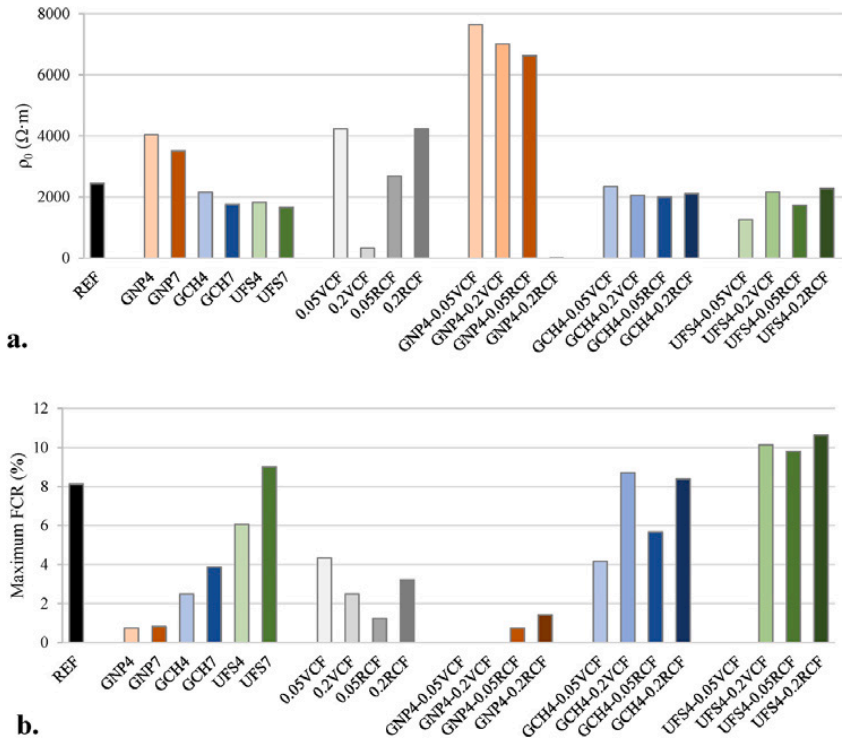

Fig. 13. Piezoresistive properties of different mortars: electrical resistivity ρ_0 (a) and FCR (b).

composite showing the max FCR, GF and SS is that containing UFS, especially at the highest dosage (UFS7) (Fig. 13b and Table 5). On the other hand, the single addition of GCH leads to a less piezoresistive mortar than UFS in terms of FCR, GF and SS (Fig. 13b and Table 5). Concerning fibers, neither VCF nor RCF alone seem to be highly effective to increase the piezoresistive behavior of mortars. On the other hand, if fibers are combined with fillers, the best piezoresistivity parameters are obtained by those containing UFS and RCF at the highest dosages where the variation in resistivity under strain is the greatest (GF = 1415). Only slightly lower values are achieved by the GCH-0.2VCF mixture. Mortars containing GNP or GNP with CF show the highest DC resistivity even if literature

Table 5
Piezoresistive properties of different mortars: maximum strain ε, GF and SS.

Mixtures	max. Strain (με)	GF (–)	SS (MPa^{-1})
REF	69	1149	$5.2 \cdot 10^{-3}$
GNP4	84	89	$0.5 \cdot 10^{-3}$
GNP7	97	85	$0.5 \cdot 10^{-3}$
GCH4	61	407	$1.6 \cdot 10^{-3}$
GCH7	78	493	$2.5 \cdot 10^{-3}$
UFS4	57	1056	$3.9 \cdot 10^{-3}$
UFS7	68	1329	$5.8 \cdot 10^{-3}$
0.05VCF	67	651	$2.8 \cdot 10^{-3}$
0.2VCF	75	329	$1.6 \cdot 10^{-3}$
0.05RCF	76	163	$0.8 \cdot 10^{-3}$
0.2RCF	67	480	$2.1 \cdot 10^{-3}$
GNP4-0.05VCF	85	–	–
GNP4-0.2VCF	83	–	–
GNP4-0.05RCF	83	90	$0.5 \cdot 10^{-3}$
GNP4-0.2RCF	87	151	$0.9 \cdot 10^{-3}$
GCH4-0.05VCF	71	584	$2.7 \cdot 10^{-3}$
GCH4-0.2VCF	77	1128	$5.6 \cdot 10^{-3}$
GCH4-0.05RCF	69	822	$3.6 \cdot 10^{-3}$
GCH4-0.2RCF	80	1043	$5.4 \cdot 10^{-3}$
UFS4-0.05VCF	90	–	–
UFS4-0.2VCF	72	1409	$6.5 \cdot 10^{-3}$
UFS4-0.05RCF	78	1256	$6.3 \cdot 10^{-3}$
UFS4-0.2RCF	75	1415	$6.8 \cdot 10^{-3}$

generally reports low values in AC measurements [69]. This discrepancy is because the DC resistance is comparable to AC impedance measured toward low frequencies, when the resistance of the matrix (R_M) gives the highest contribution [104]. In this range, the electronic contribution of GNP is not visible because it is detectable at high frequencies [66], whereas the resistivity of the binder phase is very high, due to the presence of macropores in the hardened specimens (Fig. 10) caused by GNP agglomeration, segregation phenomena, and air trapping in the fresh mix (Fig. 7). On the contrary, GCH and UFS lead to a refinement of the microstructure of mortars, decreasing the DC resistivity compared to REF. Fig. 15 shows the DC electrical behavior of some mortars with GNP under stress where the change in resistivity cannot be correlated with deformation (no piezoresistive properties). It is worthy to note that the GNP4-0.2RCF mix shows extremely low DC resistivity (Fig. 13a) confirming the optimal dispersion of the additions within this composite, where the electronic paths overcome the ionic conduction of the matrix [56]. The FCR, GF and SS of this mixture (2.2%, 232, and $1.4 \cdot 10^{-3}$, respectively) are much lower than those of GCH and UFS mortars, but the relationship between FCR and strain is the best (Fig. 14g) thanks to the low data dispersion. Therefore, the results of the present work have demonstrated that a lower electrical resistivity of cement-based composites does not always lead to higher piezoresistive parameters as FCR, GF and SS, but to a lower dispersion of measured data [73,105] with a better relationship between FCR and strain. High-conductive mortars exhibit a piezoresistive behavior similar to a strain gauge, i.e., a change in resistivity almost linear with deformation with a very low data dispersion (Fig. 14g).

4. Conclusions

In this work, the effect of commercial carbon-based fillers and fibers (GNP and VCF) on the mechanical, durability, electrical and piezoresistive behavior of structural mortars were compared to those of fillers and fibers from industrial by-products (GCH, UFS, and RCF). The carbon-based fillers were added at 4 and 7% by binder mass, whereas the carbon fibers at 0.05 and 0.2% by mortar volume.

The results showed that.

- GCH and UFS increase mortars fluidity. On the contrary, the hydrophobicity of GNP leads to segregation phenomena while CF addition does not have a significant effect on fresh mortars.
- On average, only GCH and UFS increase mortars mechanical strength, up to about +25% and +10% for R_f and R_c, respectively, regardless of the percentage addition. At the adopted dosages, the single VCF or RCF addition does not give any noticeable effect on mechanical strength. GNP reduces mortars mechanical strength owing to the presence of macropores formed during the casting phase.

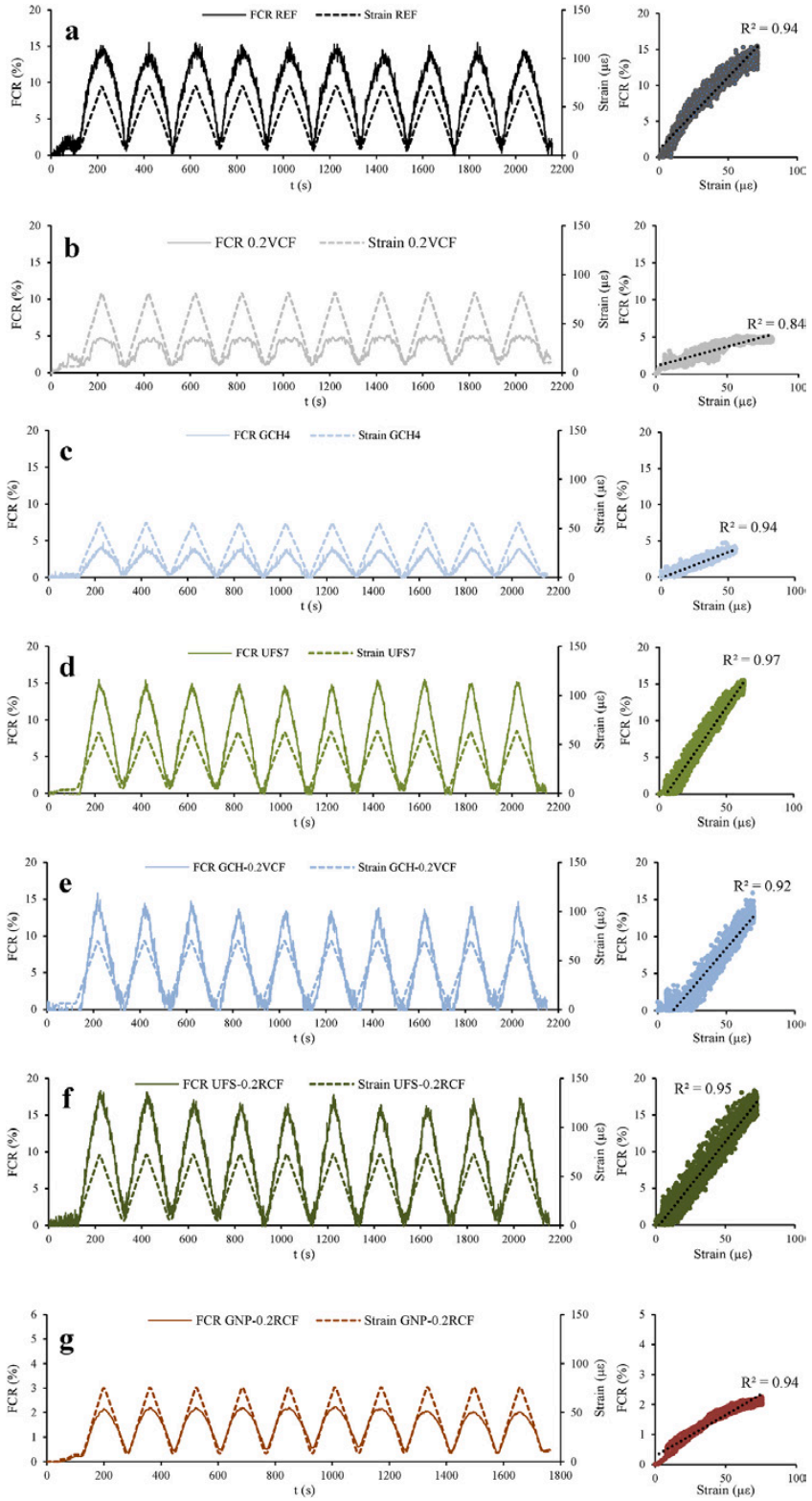

Fig. 14. FCR and strain vs. time (left) and FCR vs. strain (right) of mortars in 10 load cycles: a) REF, b) 0.2VCF, c) GCH4, d) UFS7, e) GCH-0.2VCF, f) UFS-0.2RCF, g) GNP-0.2RCF.

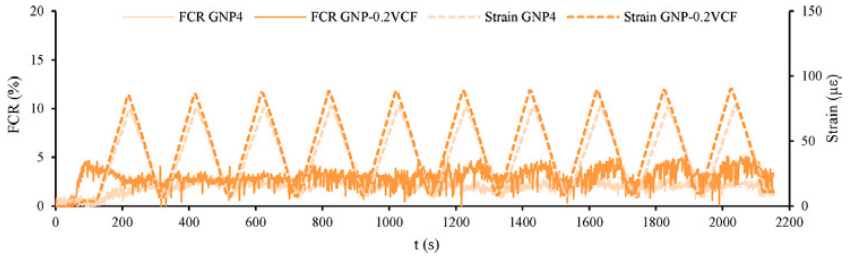

Fig. 15. FCR and strain vs. time of high-DC resistivity mortars: GNP4 and GNP-0.2VCF.

- GCH and UFS refine the microstructure decreasing the total pore volume up to 9 and 11%, respectively. Also CF reduce the total pores volume (up to 20%) regardless of their type and quantity. GNP decreases the volume of micropores but increase that of macropores.
- Both commercial and recycled fillers reduce water penetration in the composites. All mortars show lower C values (up to −27%) than the plain mortar. Moreover, GNP and UFS counteract the rising water during the first 2 days of exposure, but for longer time of exposure the final quantity of absorbed water is similar for all mixes.
- From the DC piezoresistivity tests, mortars with UFS, UFS with CF, and GCH with CF show the highest piezoresistive parameters. FCR values up to 18% are measured at the point of maximum load in the UFS4-0.2RCF mortar, with a GF of 1415, a SS of $6.8{\cdot}10^{-3}$, and a good reading repeatability. Notable results are also shown by UFS7 and GCH-0.2VCF, with GF values of 1329 and 1128, respectively. The GNP4-0.2RCF mortar with the lowest resistivity does not show the highest piezoresistive parameters (FCR, GF, SS) but the best relationship between FCR and strain due to the lowest data dispersion.

This research work confirms the better mechanical performance, durability in terms of capillary water absorption as well as self-sensing behavior for composites containing GCH, UFS and RCF compared to those prepared with GNP and VCF. This promotes new options for both the recycling/valorization of these industrial by-products also in multifunctional self-sensing cement-based materials. As a matter of fact, these cost-effective and sustainable additions allow the use of cheaper instrumentation for SHM thanks to the lower electrical resistivity and the better relationship between FCR and strain.

CRediT authorship contribution statement

Alberto Belli: Conceptualization, Methodology, Software, Validation, Formal analysis, Investigation, Data curation, Writing – original draft. **Alessandra Mobili:** Conceptualization, Methodology, Validation, Data curation, Writing – review & editing. **Tiziano Bellezze:** Conceptualization, Data curation, Resources, Writing - review & editing, Supervision. **Paulo B. Cachim:** Conceptualization, Resources, Writing - review & editing, Supervision. **Francesca Tittarelli:** Conceptualization, Resources, Writing - review & editing, Supervision.

Declaration of competing interest

The authors declare that they have no known competing financial interests or personal relationships that could have appeared to influence the work reported in this paper.

Data availability

Data will be made available on request.

Acknowledgements

The authors wish to thank STW GmbH for virgin carbon fibers and Apply Carbon SA for recycled carbon fibers kindly offered for this work. The authors wish to thank also LA.BO S.r.l. for the used foundry sand kindly offered for this work.

References

[1] D.D.L. Chung, Electrically conductive cement-based materials, Adv. Cem. Res. 4 (2004) 167–176, https://doi.org/10.1680/adcr.2004.16.4.167.
[2] S. Wen, D.D.L. Chung, Piezoresistivity in continuous carbon fiber cement-matrix composite, Cem. Concr. Res. 29 (1999) 445–449, https://doi.org/10.1016/S0008-8846(98)00211-7.
[3] D.D.L. Chung, Carbon materials for structural self-sensing, electromagnetic shielding and thermal interfacing, Carbon N. Y. 50 (2012) 3342–3353, https://doi.org/10.1016/j.carbon.2012.01.031.
[4] Y. Liu, F. Presuel, Normalization of temperature effect on concrete resistivity by method using Arrhenius Law, ACI Mater. J. 111 (2014) 433–442, https://doi.org/10.14359/51686725.
[5] P. Azarsa, R. Gupta, Electrical resistivity of concrete for durability evaluation: a review, Adv. Mater. Sci. Eng. 2017 (2017), https://doi.org/10.1155/2017/8453095.
[6] K. Osterminski, R.B. Polder, P. Schießl, Long term behaviour of the resistivity of concrete, Heron 57 (2012) 211–230.
[7] X. Dérobert, J.F. Lataste, J. Balayssac, S. Laurens, Evaluation of chloride contamination in concrete using electromagnetic non-destructive testing methods, NDT E Int. 89 (2017) 19–29, https://doi.org/10.1016/j.ndteint.2017.03.006.

[8] M. Saleem, M. Shameem, S.E. Hussain, M. Maslehuddint, Effect of moisture, chloride and sulphate contamination on the electrical resistivity Portland cement concrete, Constr. Build. Mater. 10 (1996) 209–214.
[9] A.V. Saetta, B.A. Schrefler, R.V. Vitaliani, The carbonation of concrete and the mechanism of moisture, heat and carbon dioxide flow through porous materials, Cem. Concr. Res. 23 (1993) 761–772, https://doi.org/10.1016/0008-8846(93)90030-D.
[10] J.F. Lataste, C. Sirieix, D. Breysse, M. Frappa, Electrical resistivity measurement applied to cracking assessment on reinforced concrete structures in civil engineering, NDT E Int. 36 (2003) 383–394, https://doi.org/10.1016/S0963-8695(03)00013-6.
[11] A. Lübeck, A.L.G. Gastaldini, D.S. Barin, H.C. Siqueira, Compressive strength and electrical properties of concrete with white Portland cement and blast-furnace slag, Cem. Concr. Compos. 34 (2012) 392–399, https://doi.org/10.1016/j.cemconcomp.2011.11.017.
[12] S. Wen, D.D.L. Chung, Piezoresistivity-based strain sensing in carbon fiber-reinforced cement, ACI Mater. J. 104 (2007) 171–179.
[13] E. García-Macías, A. D'Alessandro, R. Castro-Triguero, D. Pérez-Mira, F. Ubertini, Micromechanics modeling of the uniaxial strain-sensing property of carbon nanotube cement-matrix composites for SHM applications, Compos. Struct. 163 (2017) 195–215, https://doi.org/10.1016/j.compstruct.2016.12.014.
[14] F. Rajabipour, J. Weiss, Electrical conductivity of drying cement paste, Mater. Struct. 40 (2007) 1143–1160, https://doi.org/10.1617/s11527-006-9211-z.
[15] Y. Wang, Y. Wang, B. Han, B. Wan, G. Cai, Z. Li, Strain monitoring of concrete components using embedded carbon nanofibers/epoxy sensors, Constr. Build. Mater. 186 (2018) 367–378, https://doi.org/10.1016/j.conbuildmat.2018.07.147.
[16] M.-J. Lim, H.K. Lee, I.-W. Nam, H.-K. Kim, Carbon nanotube/cement composites for crack monitoring of concrete structures, Compos. Struct. 180 (2017) 741–750, https://doi.org/10.1016/j.compstruct.2017.08.042.
[17] S.-J. Lee, I. You, G. Zi, D.-Y. Yoo, Experimental investigation of the piezoresistive properties of cement composites with hybrid carbon fibers and nanotubes, Sensors 17 (2017), https://doi.org/10.3390/s17112516.
[18] K. Ogi, T. Shinoda, M. Mizui, Strength in concrete reinforced with recycled CFRP pieces, Compos. Part A Appl. Sci. Manuf. 36 (2005) 893–902, https://doi.org/10.1016/j.compositesa.2004.12.009.
[19] A. Mobili, G. Cosoli, T. Bellezze, G.M. Revel, F. Tittarelli, Use of gasification char and recycled carbon fibres for sustainable and durable low-resistivity cement-based composites, J. Build. Eng. 50 (2022), 104237, https://doi.org/10.1016/j.jobe.2022.104237.
[20] T. Oey, A. Kumar, J.W. Bullard, N. Neithalath, G. Sant, The filler effect: the influence of filler content and surface area on cementitious reaction rates, J. Am. Ceram. Soc. 96 (2013) 1978–1990, https://doi.org/10.1111/jace.12264.
[21] L. Fiala, J. Toman, J. Vodička, V. Ráček, Experimental study on electrical properties of steel-fibre reinforced concrete, Procedia Eng. 151 (2016) 241–248, https://doi.org/10.1016/J.PROENG.2016.07.362.
[22] E. Teomete, O.I. Kocyigit, Tensile strain sensitivity of steel fiber reinforced cement matrix composites tested by split tensile test, Constr. Build. Mater. Complete (2013) 962–968, https://doi.org/10.1016/J.CONBUILDMAT.2013.05.095.
[23] D.-L. Nguyen, M. Ngoc-Tra Lam, D.-J. Kim, J. Song, Direct tensile self-sensing and fracture energy of steel-fiber-reinforced concretes, Compos. Part B Eng. 183 (2020), 107714, https://doi.org/10.1016/j.compositesb.2019.107714.
[24] D.L. Nguyen, J. Song, C. Manathamsombat, D.J. Kim, Comparative electromechanical damage-sensing behaviors of six strain-hardening steel fiber-reinforced cementitious composites under direct tension, Compos. Part B Eng. 69 (2015) 159–168, https://doi.org/10.1016/j.compositesb.2014.09.037.
[25] B.G. Han, B.Z. Han, X. Yu, B.G. Han, B.Z. Han, X. Yu, Experimental study on the contribution of the quantum tunneling effect to the improvement of the conductivity and piezoresistivity of a nickel powder-filled cement-based composite, SMaS 18 (2009), 065007, https://doi.org/10.1088/0964-1726/18/6/065007.
[26] P.-W. Chen, D.D.L. Chung, Carbon-fiber-reinforced Concrete Smart Structures Capable of Nondestructive Flaw Detection, 1993, pp. 445–453, https://doi.org/10.1117/12.148502, 10.1117/12.148502. 1916.
[27] A. Belli, A. Mobili, T. Bellezze, F. Tittarelli, Commercial and recycled carbon/steel fibers for fiber-reinforced cement mortars with high electrical conductivity, Cem. Concr. Compos. 109 (2020), 103569, https://doi.org/10.1016/j.cemconcomp.2020.103569.
[28] N. Banthia, S. Djeridane, M. Pigeon, Electrical resistivity of carbon and steel micro-fiber reinforced cements, Cem. Concr. Res. 22 (1992) 804–814, https://doi.org/10.1016/0008-8846(92)90104-4.
[29] D.D.L. Chung, Dispersion of short fibers in cement, J. Mater. Civ. Eng. 17 (2005) 379–383, https://doi.org/10.1061/(ASCE)0899-1561(2005)17:4(379).
[30] P. Xie, P. Gu, J.J. Beaudoin, Electrical percolation phenomena in cement composites containing conductive fibres, J. Mater. Sci. 31 (1996) 4093–4097, https://doi.org/10.1007/BF00352673.
[31] R.M. Chacko, N. Banthia, A.A. Mufti, Carbon-fiber-reinforced cement-based sensors, Can. J. Civ. Eng. 34 (2007) 284–290, https://doi.org/10.1139/l06-092.
[32] M. Chiarello, R. Zinno, Electrical conductivity of self-monitoring CFRC, Cem. Concr. Compos. 27 (2005) 463–469, https://doi.org/10.1016/j.cemconcomp.2004.09.001.
[33] A. Al-Dahawi, O. Öztürk, F. Emami, G. Yildirim, M. Şahmaran, Effect of mixing methods on the electrical properties of cementitious composites incorporating different carbon-based materials, Constr. Build. Mater. 104 (2016) 160–168, https://doi.org/10.1016/j.conbuildmat.2015.12.072.
[34] J. Donnini, T. Bellezze, V. Corinaldesi, Mechanical, electrical and self-sensing properties of cementitious mortars containing short carbon fibers, J. Build. Eng. 20 (2018) 8–14, https://doi.org/10.1016/j.jobe.2018.06.011.
[35] S. Wen, D.D.L. Chung, Partial replacement of carbon fiber by carbon black in multifunctional cement-matrix composites, Carbon N. Y. 45 (2007) 505–513, https://doi.org/10.1016/j.carbon.2006.10.024.
[36] S. Wen, D.D.L. Chung, Uniaxial tension in carbon fiber reinforced cement, sensed by electrical resistivity measurement in longitudinal and transverse directions, Cem. Concr. Res. 30 (2000) 1289–1294, https://doi.org/10.1016/S0008-8846(00)00304-5.
[37] R. Merli, M. Preziosi, A. Acampora, M.C. Lucchetti, E. Petrucci, Recycled fibers in reinforced concrete: a systematic literature review, J. Clean. Prod. 248 (2020), 119207, https://doi.org/10.1016/j.jclepro.2019.119207.
[38] H. Nguyen, V. Carvelli, T. Fujii, K. Okubo, Cement mortar reinforced with reclaimed carbon fibres, CFRP waste or prepreg carbon waste, Constr. Build. Mater. 126 (2016) 321–331, https://doi.org/10.1016/j.conbuildmat.2016.09.044.
[39] M. Mastali, A. Dalvand, The impact resistance and mechanical properties of self-compacting concrete reinforced with recycled CFRP pieces, Compos. Part B Eng. 92 (2016) 360–376, https://doi.org/10.1016/j.compositesb.2016.01.046.
[40] J.-L. Le, H. Du, S.D. Pang, Use of 2D Graphene Nanoplatelets (GNP) in cement composites for structural health evaluation, Compos. Part B Eng. 67 (2014) 555–563, https://doi.org/10.1016/j.compositesb.2014.08.005.
[41] H. Du, S.D. Pang, Mechanical Response and strain sensing of cement composites added with graphene nanoplatelet under tension, in: K. Sobolev, V. Shah (Eds.), Nanotechnol. Constr., Springer, Cham, 2015, pp. 377–382, https://doi.org/10.1007/978-3-319-17088-6.
[42] Q. Liu, Q. Xu, Q. Yu, R. Gao, T. Tong, Experimental investigation on mechanical and piezoresistive properties of cementitious materials containing graphene and graphene oxide nanoplatelets, Constr. Build. Mater. 127 (2016) 565–576, https://doi.org/10.1016/j.conbuildmat.2016.10.024.
[43] D.D.L. Chung, Carbon Composites: Composites with Carbon Fibers, Nanofibers, and Nanotubes: Second Edition, Carbon Compos. Compos. With Carbon Fibers, second ed., Nanofibers, Nanotub, 2016, pp. 1–682.
[44] H.K. Kim, I.W. Nam, H.K. Lee, Enhanced effect of carbon nanotube on mechanical and electrical properties of cement composites by incorporation of silica fume, Compos. Struct. 107 (2014) 60–69, https://doi.org/10.1016/j.compstruct.2013.07.042.
[45] M.S. Konsta-Gdoutos, C.A. Aza, Self sensing carbon nanotube (CNT) and nanofiber (CNF) cementitious composites for real time damage assessment in smart structures, Cem. Concr. Compos. 53 (2014) 162–169, https://doi.org/10.1016/j.cemconcomp.2014.07.003.
[46] J. Zhang, Y. Ke, J. Zhang, Q. Han, B. Dong, Cement paste with well-dispersed multi-walled carbon nanotubes: mechanism and performance, Constr. Build. Mater. 262 (2020), 120746, https://doi.org/10.1016/j.conbuildmat.2020.120746.
[47] M. Jung, J. Park, S. Hong, J. Moon, Electrically cured ultra-high performance concrete (UHPC) embedded with carbon nanotubes for field casting and crack sensing, Mater. Des. 196 (2020), 109127, https://doi.org/10.1016/j.matdes.2020.109127.
[48] J. Kolosnjaj, H. Szwarc, F. Moussa, Bio-Applications of Nanoparticles, Adv. Exp. Med. Biol. 620 (2007) 181–204.

[49] J. Le, S. Pang, H. Du, Using graphite nanoplatelet reinforced cementitious composites as a self-sensing material: theory and experiments, in: EMI 2013 Conf., 2013, pp. 4–7.
[50] H. Du, S. Pang, S. Quek, Transport properties of cement mortar with graphite nanoplatelet, ICCE- 20 (2012) 22–28.
[51] S. Huang, Multifunctional Graphite Nanoplatelets (GNP) Reinforced Cementitious Composites, University of Singapore, 2012.
[52] S. Sun, B. Han, S. Jiang, X. Yu, Y. Wang, H. Li, J. Ou, Nano graphite platelets-enabled piezoresistive cementitious composites for structural health monitoring NGPs, Constr. Build. Mater. 136 (2017) 314–328, https://doi.org/10.1016/j.conbuildmat.2017.01.006.
[53] M. Mahoutian, A.S. Lubell, V. Bindiganavile, Effect of powdered activated carbon on the air void characteristics of concrete containing fly ash, Constr. Build. Mater. 80 (2015) 84–91.
[54] C.-K. Leong, D.D.L. Chung, Carbon Black Dispersions and Carbon-Silver Combinations as Thermal Pastes that Surpass Commercial Silver and Ceramic Pastes in Providing High Thermal Contact Conductance, 2004, https://doi.org/10.1016/j.carbon.2004.05.013.
[55] C.-K. Leong, Y. Aoyagi, D.D.L. Chung, Carbon Black Pastes as Coatings for Improving Thermal Gap-Filling Materials, 2005, https://doi.org/10.1016/j.carbon.2005.09.002.
[56] A.O. Monteiro, P.B. Cachim, P.M.F.J. Costa, Self-sensing piezoresistive cement composite loaded with carbon black particles, Cem. Concr. Compos. 81 (2017) 59–65, https://doi.org/10.1016/j.cemconcomp.2017.04.009.
[57] R. Siddique, A. Mehta, Effect of carbon nanotubes on properties of cement mortars, Constr. Build. Mater. 50 (2014) 116–129, https://doi.org/10.1016/j.conbuildmat.2013.09.019.
[58] A. Mohammed, J.G. Sanjayan, W.H. Duan, A. Nazari, Incorporating graphene oxide in cement composites: a study of transport properties, Constr. Build. Mater. 84 (2015) 341–347, https://doi.org/10.1016/j.conbuildmat.2015.01.083.
[59] P.-W. Chen, D.D.L. Chung, Carbon fiber reinforced concrete as an IntrinsicallySmart concrete for damage assessment duringStatic and Dynamic loading, Mater. J. 93 (1996) 341–350, https://doi.org/10.14359/9820.
[60] S. Chuah, Z. Pan, J.G. Sanjayan, C.M. Wang, W.H. Duan, Nano reinforced cement and concrete composites and new perspective from graphene oxide, Constr. Build. Mater. 73 (2014) 113–124, https://doi.org/10.1016/j.conbuildmat.2014.09.040.
[61] F. Pacheco-Torgal, S. Jalali, Nanotechnology: Advantages and drawbacks in the field of construction and building materials, Constr. Build. Mater. 25 (2011) 582–590, https://doi.org/10.1016/j.conbuildmat.2010.07.009.
[62] E. Shamsaei, F.B. de Souza, X. Yao, E. Benhelal, A. Akbari, W. Duan, Graphene-based nanosheets for stronger and more durable concrete: a review, Constr. Build. Mater. 183 (2018) 642–660, https://doi.org/10.1016/j.conbuildmat.2018.06.201.
[63] M. Zhang, Y. Ma, Y. Zhu, J. Che, Y. Xiao, Two-dimensional transparent hydrophobic coating based on liquid-phase exfoliated graphene fluoride, Carbon N. Y. 63 (2013) 149–156, https://doi.org/10.1016/j.carbon.2013.06.066.
[64] B. Bhardwaj, P. Kumar, Waste foundry sand in concrete: a review, Constr. Build. Mater. 156 (2017) 661–674, https://doi.org/10.1016/j.conbuildmat.2017.09.010.
[65] A. Mobili, A. Belli, C. Giosuè, M. Pierpaoli, L. Bastianelli, A. Mazzoli, M. Letizia, T. Bellezze, F. Tittarelli, Mechanical, durability, depolluting and electrical properties of multifunctional mortars prepared with commercial or waste carbon-based fillers, Constr. Build. Mater. 283 (2021), 122768, https://doi.org/10.1016/j.conbuildmat.2021.122768.
[66] A. Mobili, C. Giosuè, T. Bellezze, G.M. Revel, F. Tittarelli, Gasification char and used foundry sand as alternative fillers to graphene nanoplatelets for electrically conductive mortars with and without virgin/recycled carbon fibres, Appl. Sci. 11 (2021) 50, https://doi.org/10.3390/app11010050.
[67] V. Benedetti, F. Patuzzi, M. Baratieri, Gasification char as a potential substitute of activated carbon in adsorption applications, Energy Proc. 105 (2017) 712–717, https://doi.org/10.1016/j.egypro.2017.03.380.
[68] M. Chen, P. Gao, F. Geng, L. Zhang, H. Liu, Mechanical and smart properties of carbon fiber and graphite conductive concrete for internal damage monitoring of structure, Constr. Build. Mater. 142 (2017) 320–327, https://doi.org/10.1016/j.conbuildmat.2017.03.048.
[69] A. Belli, A. Mobili, T. Bellezze, P.B. Cachim, F. Tittarelli, Self-sensing mortars with recycled carbon-based fillers and fibers, ACI Spec. Publ. SP- 355 (2022) 115–132.
[70] G.M. Kim, H.N. Yoon, H.K. Lee, Autogenous shrinkage and electrical characteristics of cement pastes and mortars with carbon nanotube and carbon fiber, Constr. Build. Mater. 177 (2018) 428–435, https://doi.org/10.1016/j.conbuildmat.2018.05.127.
[71] A. Belli, A. Mobili, T. Bellezze, F. Tittarelli, P.B. Cachim, Evaluating the self-sensing ability of cement mortars manufactured with graphene nanoplatelets, virgin or recycled carbon fibers through piezoresistivity tests, Sustainability 10 (2018) 4013, https://doi.org/10.3390/su10114013.
[72] European Committee for Standardization, Methods of Test for Mortar for Masonry - Part 6: Determination of Bulk Density of Fresh Mortar (EN 1015-6:1998/A1:2006), 2006.
[73] A.O. Monteiro, A. Loredo, P.M.F.J. Costa, M. Oeser, P.B. Cachim, A pressure-sensitive carbon black cement composite for traffic monitoring, Constr. Build. Mater. 154 (2017) 1079–1086, https://doi.org/10.1016/j.conbuildmat.2017.08.053.
[74] European Committee for Standardization, Methods of Test for Mortar for Masonry - Part 11: Determination of Flexural and Compressive Strength of Hardened Mortar (EN 1015-11:1999/A1:2006), 2006.
[75] European Committee for Standardization, Methods of Test for Mortar for Masonry - Part 3: Determination of Consistence of Fresh Mortar, 2006 (by flow table) (EN 1015-3:1999/A2:2006).
[76] European Committee for Standardization, Methods of Test for Mortar for Masonry - Part 18: Determination of Water Absorption Coefficient Due to Capillary Action of Hardened Mortar (EN 1015-18:2002), 2002.
[77] European Committee for Standardization, Conservation of Cultural Property - Test Methods - Determination of Water Absorption by Capillarity (EN 15801:2009), 2009.
[78] B. Han, X. Guan, J. Ou, Electrode design, measuring method and data acquisition system of carbon fiber cement paste piezoresistive sensors, Sensors Actuators, A Phys. 135 (2007) 360–369, https://doi.org/10.1016/j.sna.2006.08.003.
[79] G. Faneca, I. Segura, J.M. Torrents, A. Aguado, Development of conductive cementitious materials using recycled carbon fibres, Cem. Concr. Compos. 92 (2018) 135–144, https://doi.org/10.1016/j.cemconcomp.2018.06.009.
[80] S. Wen, D.D.L. Chung, Piezoresistivity-based strain sensing in carbon fiber- reinforced cement, ACI Mater. J. 104 (2007) 171–179.
[81] A.O. Monteiro, P.B. Cachim, P.M.F.J. Costa, Electrical properties of cement-based composites containing carbon black particles, Mater. Today Proc. 2 (2015) 193–199, https://doi.org/10.1016/j.matpr.2015.04.021.
[82] A. Belli, A. Mobili, T. Bellezze, F. Tittarelli, P.B. Cachim, Piezoresistive behavior of mortars loaded with graphene and carbon fibers for the development of self-sensing composites, in: Adv. Trends Eng. Sci. Technol. III- Proc. 3rd Int. Conf. Eng. Sci. Technol., Taylor & Francis Group, 2019, pp. 37–42.
[83] F.J. Baeza, O. Galao, E. Zornoza, P. Garcés, Effect of aspect ratio on strain sensing capacity of carbon fiber reinforced cement composites, Mater. Des. 51 (2013) 1085–1094, https://doi.org/10.1016/j.matdes.2013.05.010.
[84] Y. Guney, Y. Dursun, M. Yalcin, A. Tuncan, S. Donmez, Re-usage of waste foundry sand in high-strength concrete, Waste Manag. 30 (2010) 1705–1713, https://doi.org/10.1016/j.wasman.2010.02.018.
[85] R. Siddique, Utilization of industrial by-products in concrete, Procedia Eng. 95 (2014) 335–347, https://doi.org/10.1016/j.proeng.2014.12.192.
[86] A. Mazzoli, V. Corinaldesi, J. Donnini, C. Di Perna, D. Micheli, A. Vricella, R. Pastore, L. Bastianelli, F. Moglie, V. Mariani Primiani, Effect of graphene oxide and metallic fibers on the electromagnetic shielding effect of engineered cementitious composites, J. Build. Eng. 18 (2018) 33–39, https://doi.org/10.1016/j.jobe.2018.02.019.
[87] P. Faria, P. Duarte, D. Barbosa, I. Ferreira, New composite of natural hydraulic lime mortar with graphene oxide, Constr. Build. Mater. 156 (2017) 1150–1157, https://doi.org/10.1016/j.conbuildmat.2017.09.072.
[88] P. Garcés, E. Zornoza, E.G. Alcocel, Ó. Galao, L.G. Andión, Mechanical properties and corrosion of CAC mortars with carbon fibers, Constr. Build. Mater. 34 (2012) 91–96, https://doi.org/10.1016/j.conbuildmat.2012.02.020.

[89] B. Han, L. Zhang, C. Zhang, Y. Wang, X. Yu, J. Ou, Reinforcement effect and mechanism of carbon fibers to mechanical and electrically conductive properties of cement-based materials, Constr. Build. Mater. 125 (2016) 479–489, https://doi.org/10.1016/j.conbuildmat.2016.08.063.
[90] E. Berodier, K. Scrivener, Understanding the filler effect on the nucleation and growth of C-S-H, J. Am. Ceram. Soc. 97 (2014) 3764–3773, https://doi.org/10.1111/jace.13177.
[91] R. Mrad, G. Chehab, Mechanical and microstructure properties of Biochar-based mortar: an internal curing agent for PCC, Sustainability 11 (2020) 2491, https://doi.org/10.3390/su11092491.
[92] X. Kang, X. Zhu, J. Liu, X. Shu, Y. Huang, J. Qian, Dissolution and precipitation behaviours of graphene oxide/tricalcium silicate composites, Compos. Part B. 186 (2020), 107800, https://doi.org/10.1016/j.compositesb.2020.107800.
[93] X. Zhu, X. Kang, J. Deng, K. Yang, L. Yu, C. Yang, A comparative study on shrinkage characteristics of graphene oxide (GO) and graphene nanoplatelets (GNPs) modified alkali-activated slag cement composites, Mater. Struct. 54 (2022) 1–15, https://doi.org/10.1617/s11527-021-01695-w.
[94] J. Foldyna, V. Foldyna, M. Zeleňák, Dispersion of carbon nanotubes for application in cement composites, Procedia Eng. 149 (2016) 94–99, https://doi.org/10.1016/j.proeng.2016.06.643.
[95] K. Gong, S.M. Asce, Z. Pan, A.H. Korayem, D. Ph, L. Qiu, D. Li, F. Collins, C.M. Wang, W.H. Duan, a M. Asce, Reinforcing effects of graphene oxide on Portland cement paste, J. Mater. Civ. Eng. 27 (2014) 1–6, https://doi.org/10.1061/(ASCE)MT.1943-5533.0001125.
[96] R. Kumar, B. Bhattacharjee, Porosity, pore size distribution and in situ strength of concrete, Cem. Concr. Res. 33 (2003) 155–164, https://doi.org/10.1016/S0008-8846(02)00942-0.
[97] V.L. Bonavetti, V.F. Rahhal, E.F. Irassar, Studies on the carboaluminate formation in limestone filler-blended cements, Cem. Concr. Res. 31 (2001) 853–859, https://doi.org/10.1016/S0008-8846(01)00491-4.
[98] H. Moosberg-Bustnes, B. Lagerblad, E. Forssberg, The function of fillers in concrete, Mater. Struct. 37 (2004) 74–81, https://doi.org/10.1617/13694.
[99] H. Nguyen, T. Fujii, K. Okubo, V. Carvelli, Cement mortar reinforced with recycled carbon fiber and CFRP waste, ECCM 2016 - Proceeding 17th, Eur. Conf. Compos. Mater. (2016).
[100] Z. Pan, L. He, L. Qiu, A.H. Korayem, G. Li, J.W. Zhu, F. Collins, D. Li, W.H. Duan, M.C. Wang, Mechanical properties and microstructure of a graphene oxide-cement composite, Cem. Concr. Compos. 58 (2015) 140–147, https://doi.org/10.1016/j.cemconcomp.2015.02.001.
[101] S.G. Prolongo, R. Moriche, A. Jiménez-Suárez, M. Sánchez, A. Ureña, Advantages and disadvantages of the addition of graphene nanoplatelets to epoxy resins, Eur. Polym. J. 61 (2014) 206–214, https://doi.org/10.1016/j.eurpolymj.2014.09.022.
[102] H. Du, S.D. Pang, Enhancement of barrier properties of cement mortar with graphene nanoplatelet, Cem. Concr. Res. 76 (2015) 10–19, https://doi.org/10.1016/j.cemconres.2015.05.007.
[103] H. Bilal, M. Yaqub, S.K.U. Rehman, M. Abid, R. Alyousef, H. Alabduljabbar, F. Aslam, Performance of foundry sand concrete under Ambient and Elevated temperatures, Materials 12 (2019) 2645, https://doi.org/10.3390/ma12162645.
[104] J.M. Torrents, T.O. Mason, E.J. Garboczi, Impedance spectra of fiber-reinforced cement-based composites: a modeling approach, Cem. Concr. Res. 30 (2000) 585–592, https://doi.org/10.1016/S0008-8846(00)00211-8.
[105] A.L. Pisello, A. D'Alessandro, S. Sambuco, M. Rallini, F. Ubertini, F. Asdrubali, A.L. Materazzi, F. Cotana, Multipurpose experimental characterization of smart nanocomposite cement-based materials for thermal-energy efficiency and strain-sensing capability, Sol. Energy Mater. Sol. Cells 161 (2017) 77–88, https://doi.org/10.1016/j.solmat.2016.11.030.